

PAT3D: PHYSICS-AUGMENTED TEXT-TO-3D SCENE GENERATION

Guying Lin¹ Kemeng Huang^{2,1} Michael Liu¹ Ruihan Gao¹ Hanke Chen¹ Lyuhao Chen¹
 Beijia Lu¹ Taku Komura² Yuan Liu³ Jun-Yan Zhu¹ Minchen Li^{1,4}

¹Carnegie Mellon University ²The University of Hong Kong

³The Hong Kong University of Science and Technology ⁴Genesis AI

{guyingl, mliu6, ruihang, lyuhao, beijialu}@andrew.cmu.edu,
 kmhuang@connect.hku.hk, {hankec, junyanz}@cs.cmu.edu, taku@cs.hku.hk,
 yuanly@ust.hk, minchernl@gmail.com

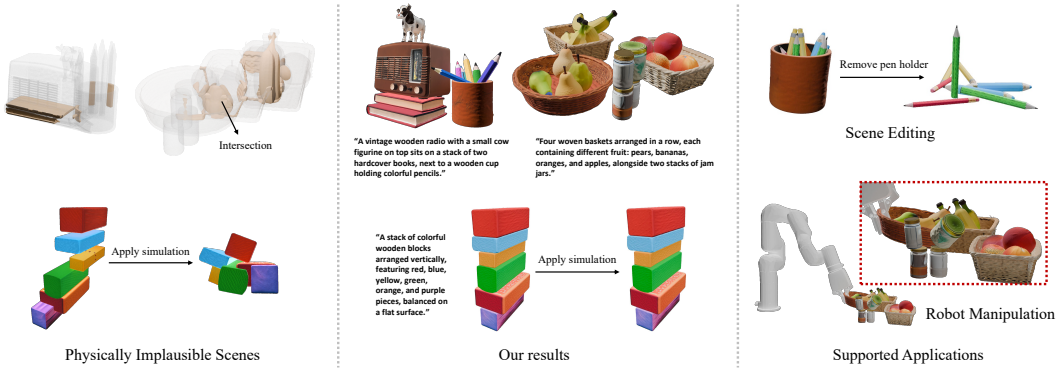


Figure 1: PAT3D is the first text-to-3D scene generation framework that produces **simulation-ready** and **intersection-free** results. The left column shows results from direct depth-based arrangements, which suffer from object interpenetrations (top) and collapse under simulation due to inconsistent layouts (bottom). The middle column presents PAT3D results, where physically valid layouts remain stable under simulation. These high-quality scenes are immediately usable for downstream applications, including scene editing and robotic manipulation (right).

ABSTRACT

We introduce PAT3D, the first physics-augmented text-to-3D scene generation framework that integrates vision-language models with physics-based simulation to produce physically plausible, simulation-ready, and intersection-free 3D scenes. Given a text prompt, PAT3D generates 3D objects, infers their spatial relations, and organizes them into a hierarchical scene tree, which is then converted into initial conditions for simulation. A differentiable rigid-body simulator ensures realistic object interactions under gravity, driving the scene toward static equilibrium without interpenetrations. To further enhance scene quality, we introduce a simulation-in-the-loop optimization procedure that guarantees physical stability and non-intersection, while improving semantic consistency with the input prompt. Experiments demonstrate that PAT3D substantially outperforms prior approaches in physical plausibility, semantic consistency, and visual quality. Beyond high-quality generation, PAT3D uniquely enables simulation-ready 3D scenes for downstream tasks such as scene editing and robotic manipulation. Code and data will be released upon acceptance.

1 INTRODUCTION

The ability to generate realistic and editable 3D scenes from natural language has broad applications across a variety of domain including virtual reality, robotics, digital twins, and content creation. Recent advances in diffusion and autoregressive generative models have significantly pushed the boundaries of text-to-3D scene generation, making it possible to synthesize high-quality object geometry and compelling visual content Lin et al. (2023); Metzer et al. (2023); Michel et al. (2022); Poole et al. (2023); Chen et al. (2025b; 2024a); Huang et al. (2024); Gao et al. (2024). However, despite these advances, existing approaches struggle to ensure that generated scenes exhibit *physical plausibility* – a critical requirement for downstream applications that demand interaction, simulation, or building a real-world correspondence.

In particular, current 3D scene generation pipelines Huang et al. (2024); Gao et al. (2024) often treat layout composition as a purely geometric problem, omitting physical reasoning entirely or using simple heuristics to prevent unfavored physical interaction such as object intersection. Due to the lack of explicit constraints from physics, this leads to common issues such as floating, unstable stacking, and incorrect support relations, ultimately limiting scene realism and usability. Earlier efforts have incorporated physical constraints to enhance single-object stability Guo et al. (2024); Chen et al. (2024c), or used video diffusion priors for plausible dynamics Zhang et al. (2024), but none of these methods address the complex spatial dependencies and contact interactions required for stable and semantically coherent multi-object scenes.

One promising direction is to integrate physics-based simulation into the scene generation process to enhance physical realism. However, this approach introduces several challenges. First, objects must be represented as individually segmented 3D meshes to enable simulation of interactions under gravity and contact forces. Applying simulation to scenes represented by a single connected mesh is ineffective, as it fails to capture interactions between objects. Second, physics-based simulation requires a well-posed initial configuration, typically free of intersections, to avoid numerical instability and unrealistic behavior Li et al. (2020). Yet, identifying such an intersection-free starting state is nontrivial. Finally, even if the simulated scene is physically plausible, it may diverge from the intended semantics described in the input text, due to the multiplicity of valid static equilibria.

To address these challenges, we propose **PAT3D**, a *physics-augmented text-to-3D scene generation* framework that integrates differentiable rigid-body contact simulation into the generation pipeline. Given a text prompt, we first synthesize a reference image to reflect the spatial relations among objects. Individual objects are then generated and coarsely positioned using vision foundation models Bochkovskii et al. (2025); Kirillov et al. (2023b); Hunyuan3D (2025). Next, a vision-language model (VLM) Hurst et al. (2024) extracts the physical dependencies between objects from the reference image, which are then organized into a scene tree. PAT3D then produces an intersection-free initial configuration from the coarsely positioned 3D scene and scene tree through physics-guided refinement. This initialization deliberately introduces small gaps along the gravity direction for objects with parent–child relations in the scene hierarchy, simplifying intersection avoidance while preserving inferred spatial relations. These gaps are later resolved through simulation, allowing objects to settle naturally under gravity and contact forces while making slight, physically plausible adjustments to their spatial relations. Finally, differentiable simulation is applied to further optimize the layout, improving semantic consistency in the resulting scene.

We validate our method on diverse, contact-rich scenes and demonstrate its effectiveness against existing state-of-the-art 3D scene generation approaches through both qualitative and quantitative evaluations under visual quality and physical plausibility metrics. We further demonstrate that our generated scenes are readily editable and interactable through simulation, enabling physically plausible scene editing and direct construction of simulation environments for policy evaluation in robotic manipulation tasks. *Our code and data will be publicly released upon acceptance.*

In summary, our main contributions include:

- We introduce **PAT3D**, the first physics-augmented text-to-3D scene generation framework that integrates vision–language models with physics-based simulation, achieving state-of-the-art physical plausibility, semantic consistency, and visual quality.
- We propose a physics-aware scene initialization module to prepare scenes for simulation. This module infers physical dependencies among objects, organizes them into a hierar-

chical scene tree, and converts the scene tree into intersection-free initial conditions for simulation.

- We develop a layout optimization strategy based on artificially time-stepped differentiable simulation, enabling efficient evaluation and differentiation of static equilibrium w.r.t initial layout.

2 RELATED WORK

Single Object Generation. Building on the success of text-to-image generation models Rombach et al. (2022); Ramesh et al. (2022); Kang et al. (2023); Yu et al. (2022), there has been rapid progress in 3D generative models conditioned on text or images. A prominent class of methods leverages 2D diffusion priors for 3D generation Poole et al. (2023); Wang et al. (2023); Lin et al. (2023); Chen et al. (2023); Metzer et al. (2023); Wang et al. (2024); Sun et al. (2024); Long et al. (2024); Michel et al. (2022), with DreamFusion Poole et al. (2023) introducing Score Distillation Sampling (SDS) to optimize 3D representations using gradients from 2D diffusion models. Subsequent works have extended SDS with multi-view diffusion models, improving both 3D generation quality and single-view reconstruction Liu et al. (2023a); Wang & Shi (2023); Shi et al. (2024); Liu et al. (2024b); Zhou & Tulsiani (2023); Liu et al. (2024a); Long et al. (2024); Shi et al. (2023); Liu et al. (2024d). Another research direction trains large-scale transformers to generate 3D shapes in a feed-forward manner Hong et al. (2024); Li et al. (2024); Xu et al. (2024b); Tochilkin et al. (2024), relying on curated, large-scale 3D asset datasets. While these models can generate visually compelling shapes, they often ignore the physical properties, such as stability, of the object, which are essential for real-world applications. To address this, recent efforts have incorporated physics-based simulation into the generation pipeline to produce self-supporting 3D objects by optimizing physical attributes such as mass distribution Guo et al. (2024); Chen et al. (2024c); Yan et al. (2024); Cai et al. (2024). Additionally, PhysDreamer Zhang et al. (2024), optimizes physical properties like Young’s modulus and initial velocity to generate dynamic motions that are both visually plausible and physically grounded, guided by video diffusion priors.

Scene Generation. While single-object generation methods produce visually appealing assets, they often lack scale awareness and spatial grounding, making scene composition challenging. The primary bottlenecks in 3D scene generation include decomposing scenes into individual assets, estimating their relative scale and pose, and ensuring physical feasibility (e.g., contact, stability). Several works address these challenges through multi-stage pipelines. Early methods such as Vilesov et al. (2023); Chen et al. (2024b); Han et al. (2024) adopt object-centric reconstruction followed by layout and geometry optimization using physical constraints or differentiable rendering. Shriram et al. (2024) lifts the scene image to 3D point clouds as a whole, inpaints occluded regions, and refines appearance using 2D diffusion priors. Recently, Large Language Models (LLMs) and VLMs are increasingly leveraged to infer spatial relations and scene structure. Gao et al. (2024) constructs a scene graph with objects as nodes and their relations as edges. Zhou et al. (2024) uses a VLM to generate a coarse layout, which is subsequently refined with rendering losses and physical constraints. Yao et al. (2025) infers a scene graph describing simplified pairwise relationships between objects, and use them to optimize object poses and scales. Wang et al. (2025) similarly leverages LLM-based reasoning to query objects’ relative sizes and physical properties, enabling more plausible scene layouts. However, none of these methods can ensure physically accurate contact handling or maintain physical stability in the generated scene. Scene-level optimization under SDS loss is commonly used for joint geometry-text alignment Zhou et al. (2025), while Huang et al. (2024) and Xu et al. (2024a) explore multi-instance and 4D compositional generation guided by spatial and trajectory priors. Other approaches incorporate physical property estimation into 3D representations, either from visual cues Zhao et al. (2024) or explicit user input Chen et al. (2025a), to support dynamic simulation or interaction Liu et al. (2024c). Recent systems such as Blender-MCP and Li et al. (2025b) integrate LLM reasoning and generative priors into graphics tools like Blender, enabling fine-grained control and interactive refinement. Sun et al. (2025) propose LayoutVLM, which uses a VLMs to generate differentiable spatial relations and jointly optimize 3D layouts in indoor scenes. However, most existing scene generation methods focus primarily on layout composition. They either omit physical reasoning altogether or incorporate only simple physics priors to prevent object interpenetration, without modeling accurate contact interactions or ensuring physically stable

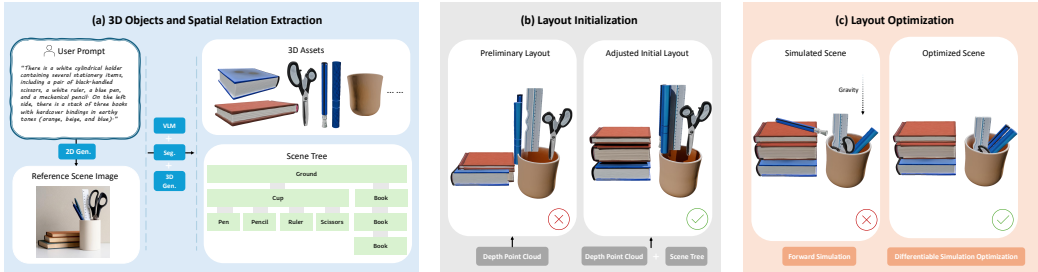


Figure 2: **Overview of our text-to-3D scene generation pipeline.** (a) Given an input text, a reference image is first generated to capture spatial relations among objects, from which 3D assets are generated using vision foundation models, and a scene tree is extracted using a VLM. (b) Assets are arranged into an initial layout using 3D priors from monocular depth estimation (left), then refined with the scene tree to produce an intersection-free configuration for simulation (right). (c) Forward simulation ensures physical plausibility but may distort semantics (left). We address this with simulation-in-the-loop optimization, enforcing semantic consistency and physical validity (right).

scene layouts. We thus address this gap by novelly augmenting text-to-3D scene generation with differentiable rigid body contact simulation.

3 METHOD

Our framework comprises three stages: *3D object and spatial relation extraction* (subsection 3.1), where 3D assets are generated from text and its spatial relation are organized into a scene tree; *layout initialization* (subsection 3.2), which first arranges generated assets using monocular depth priors obtained from reference image and uses scene tree to refine them into an intersection-free configuration; and *layout optimization* (subsection 3.3), where a simulation-in-the-loop optimization procedure is applied to ensure physical plausibility and improve semantic consistency of 3D scene.

3.1 3D OBJECT AND SPATIAL RELATION EXTRACTION

Since directly producing both 3D objects and layouts with text-to-3D models and LLMs often fails to capture complex spatial relations, we instead employ a text-to-image model to generate a reference image that guides object generation and scene tree construction. See Figure 2(a).

3.1.1 3D OBJECTS GENERATION

To generate individual objects for the scene specified by the text prompt, a VLM is queried with the reference image to obtain object class labels, and the image is segmented with Grounded-SAM Kirillov et al. (2023a); Ren et al. (2024); Liu et al. (2023b) accordingly. Based on the segmented object regions, we further prompt the VLM to generate detailed text descriptions encompassing object semantics, material, color, and orientation. These descriptions are fed into a text-to-3D pipeline Hunyuan3D (2025) to synthesize high-quality, textured 3D assets that are both semantically consistent and visually realistic.

3.1.2 SPATIAL RELATION EXTRACTION

We then extract the relative spatial relations among objects in the scene from the reference image and analyze their physical dependencies. This information provides essential guidance for intersection-free layout initialization (subsection 3.2) and subsequent optimization (subsection 3.3). Specifically, for each pair of segmented objects that appear with similar horizontal positions and adjacent vertical positions in the reference image, we prompt a VLM to infer their dependency along the gravity axis, identifying relations such as on, contain, and support. The resulting pairwise relations are then organized into a hierarchical scene tree that encodes how objects support one another under gravity. Starting with the ground as the root node, we traverse the scene and iteratively add objects as nodes in the tree. For each unvisited object that has a direct physical dependency with an existing node, we

insert it as a child of that node. This recursive process continues until all objects have been included. Additional details are provided in Algorithm 1, and an example is shown in Figure 2(a).

3.2 LAYOUT INITIALIZATION

To obtain an intersection-free and semantically consistent initial layout for the subsequent simulation-in-the-loop optimization, we first compute the translational and scaling transformations to build a preliminary layout consistent with the reference image, and then refine it using the extracted scene tree to ensure no object intersection and stronger physical constraints. See Figure 2(b).

3.2.1 PRELIMINARY LAYOUT

Our straightforward approach to arranging the objects generated in subsubsection 3.1.1 into a layout consistent with the reference image is to back-project the 2D reference image with depth estimation to obtain each object’s 3D point cloud. Scaling and translational transformations can then be computed by aligning the object’s center with the centroid of its point cloud. In practice, however, heavy occlusions in the 2D image make scaling unreliable when derived directly from partial point clouds. To address this, we first query the VLM to identify the least occluded object in the scene and use it as an anchor to compute a global scaling transformation for the entire scene. We then compute relative scaling for the other objects by prompting the VLM to inpaint occluded regions of the 2D image and estimating scaling factors from the bounding boxes of the inpainted objects. Each object’s final transformation is obtained by combining the global and relative scaling factors, followed by alignment with the projected 3D point cloud. This procedure produces the preliminary layout shown in Figure 2(b).

3.2.2 REFINED INITIAL LAYOUT

To refine the layout under physical dependency constraints and ensure non-intersection, we traverse the scene tree in a breadth-first manner and apply horizontal and vertical refinements at each node.

Horizontal refinement. We enforce two rules: (1) Parent–child: the projection of the child must lie entirely within that of the parent (e.g., fruits inside a basket); (2) Sibling: objects sharing the same parent must have non-overlapping projections (e.g., a vase, plate, and fork on a table).

Vertical refinement. Each child is lifted above the bounding box of its parent along the gravity axis, preventing intersections.

This simple strategy, compared with more complex optimization methods, efficiently resolves intersections while preserving semantic constraints, providing favorable initial conditions for simulation. The refined results are shown in Figure 2(b).

3.3 LAYOUT OPTIMIZATION

After simulation, gravity causes child objects to fall onto or into their respective parents, and sibling objects naturally adopt physically plausible poses. However, due to complex inter-object interactions, simulation alone may cause the scene to deviate from its intended semantics. To address this, we introduce a simulation-in-the-loop optimization to improve semantic consistency in the simulated scene. See Figure 2(c).

Specifically, we refine our intersection-free initialization q_0 so that the final equilibrium state q_{n+1} better aligns with the scene tree:

$$\min_{q_0} L(q_{n+1}(q_0)) \quad \text{s.t.} \quad f(q_{n+1}) = 0, \quad (1)$$

where L measures semantic inconsistency and f denotes the net force on all objects..

For each object i with container t , we define its projected bounding box on the horizontal plane as $\text{BBox}_i = \{\mathbf{p}_{\min}^i, \mathbf{p}_{\max}^i\}$. The local loss penalizes deviations of the corners of i from BBox_t :

$$l_i = d(\mathbf{p}_{\min}^i, \text{BBox}_t)^2 + d(\mathbf{p}_{\max}^i, \text{BBox}_t)^2, \quad (2)$$

where $d(\mathbf{p}, \text{BBox}) = 0$ if $\mathbf{p} \in \text{BBox}$, otherwise, d is the Euclidean distance from \mathbf{p} to the box boundary. The total loss is defined as

$$L(q_{n+1}(q_0)) = \sum_{i=1}^N l_i, \quad (3)$$

where N is the total number of objects in the scene.

Direct gradients of q_{n+1} with respect to q_0 cannot be obtained by differentiating the static equilibrium constraint $f(q_{n+1}) = 0$, since q_0 serves only as the initial guess and is not part of the constraint. Differentiating through the nonlinear solver is also prohibitively expensive. Instead, we adopt an artificial time-stepping formulation Fang et al. (2021), in which the quasi-static system gradually evolves toward equilibrium across intermediate states. This enables efficient backpropagation from q_{n+1} to q_0 via implicit differentiation at each step. See Appendix B for more details on our forward simulation method and the derivation of differentiation.

4 EXPERIMENTAL RESULTS

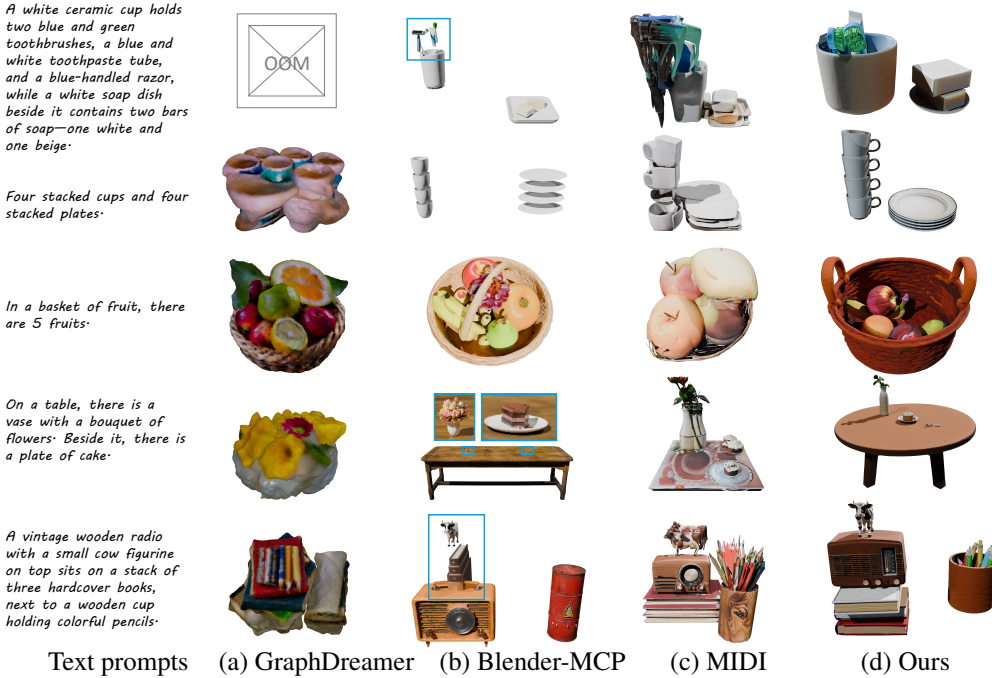


Figure 3: **Comparison to baseline methods.** The scenes are generated from our text prompts. OOM indicates out of memory.

4.1 COMPARISON

4.1.1 BASELINES

We compare our method against three baselines: GraphDreamer Gao et al. (2024), MIDI Huang et al. (2024), and Blender-MCP or ahujasid (2025). Both GraphDreamer and Blender-MCP take text prompts as input, while MIDI uses a reference image as input. To ensure a fair comparison, we provide MIDI with our scene reference image as their input.

4.1.2 DATASET

Since there is no standard benchmark for general scene generation, we construct our own test dataset consisting of 18 text prompts. Among them, 3 prompts are taken from MIDI, and 2 prompts are from

	Clip Score \uparrow	VQA Score \uparrow	Displacement \downarrow	Pene. Ratio \downarrow	Phys. Score \uparrow
GraphDreamer	27.53	0.46	0.25	61.72	40.0
Blender-MCP	28.93	0.56	1.03	14.78	47.7
MIDI	29.68	0.63	0.69	110.80	62.7
Raw layout	29.88	0.64	0.81	14.11	65.5
Scene Init.	30.77	0.70	2.91	0	34.2
Ours	31.79	0.68	0	0	88.5

Table 1: **Quantitative Evaluation.** Our method achieves the highest semantic consistency with input text prompts among all baselines, and is the only method that achieves perfect physical stability and non-intersection. We also provide ablation results: removing both layout initialization and optimization (shown as *raw layout*), and removing only layout optimization (shown as *scene init.*).

GraphDreamer. Additionally, we use an LLM to generate 13 new text prompts spanning diverse scenes. These prompts describe physical interactions between objects, including a stack of books and a basket of fruits. Additional 3D results generated by our method, in comparison with the baselines, along with corresponding text prompts and reference images, can be found on visualization website¹. Beyond these comparisons, we also present 12 more examples produced by our method in Appendix E.

4.1.3 EVALUATION METRICS

We evaluate our generated scenes using five metrics: CLIP ScoreRadford et al. (2021), VQA ScoreLin et al. (2024), Simulated Scene Displacement (D), the Ratio of Penetrating Triangle Pairs (R), and a Physical Plausibility Score. Together, these metrics measure semantic consistency, physical stability, interpenetration, and overall physical plausibility. Details of all metrics are provided in Appendix F.

4.1.4 PERFORMANCE AND DISCUSSIONS

In Figure 3, we compare PAT3D with baseline methods on five general scenes involving complex object interactions. Additional comparisons with four scenes highlighted in the MIDI and GraphDreamer are provided in Appendix E. Importantly, in PAT3D, reference image serves only to extract the complex spatial relations implied in the text prompt; the final scene does not need to remain visually consistent with the reference image.

GraphDreamer struggles to scale to larger scenes because it jointly optimizes both object geometry and scene layout through Score Distillation Sampling (SDS) Poole et al. (2023), which is highly resource-intensive. Moreover, GraphDreamer exhibits weak understanding of spatial relations in text prompts. As shown in the second, fourth, and fifth scenes of Figure 3, it often ignores spatial constraints, leading to chaotic object arrangements. Blender-MCP generates layouts with little physical realism. In the first and second scenes of Figure 3, the razor and toothbrush float above the cup, and the plate is suspended in mid-air. It also produces objects with unrealistic scales: in the fourth scene, the cake and vase appear disproportionately small compared to the table. MIDI encounters difficulties when handling scenes with complex object contact, as seen in the first, second, and fifth scenes of Figure 3, objects often appear in irregular yet tightly packed configurations. Although interpenetration is avoided, the resulting layouts are cluttered potentially because MIDI generates the entire scene in a single step, the quality of individual objects is compromised.

By contrast, our method decomposes the scene generation process, iteratively creating objects to ensure high-quality results. Leveraging VLM-based guidance together with physics simulations, PAT3D produces 3D scenes that are both physically realistic and semantically consistent, even in scenarios with complex object interactions. Quantitative comparisons are shown in Table 1. Compared to baseline methods, which frequently suffer from object intersection and floating artifacts that undermine physical plausibility, our approach consistently produces stable, penetration-free arrangements. Our method also achieves the highest semantic consistency with the input text prompts.

¹<https://3dsim-baseline-visualization.netlify.app/>

4.2 APPLICATION

Our generated simulation-ready scenes can be directly imported into a simulator for downstream applications. We demonstrate two such applications: scene editing and robotic manipulation.

4.2.1 SCENE EDITING

We demonstrate a scene editing application enabled by our framework, which supports interactive manipulation while preserving the physical plausibility of the entire scene, including object addition and deletion. By leveraging our physics-based simulation backend, the edited scene converges to a force-equilibrium state without mesh intersections. Figure 4 highlights an example showcasing object addition and deletion.



Figure 4: **Scene editing.** We demonstrate the equilibrium state after addition and deletion operations: (a) initial scene, (b) deleting a book at the bottom, (c) deleting the pen holder, (d) adding a book on top.

4.2.2 ROBOTIC MANIPULATION

Our generated scenes can be directly imported into a simulator to validate robotic manipulation policies. In Figure 5, we present two illustrative examples, a failed grasp and a successful grasp. Robotic manipulation applications impose unique requirements on scene generation: objects must be consistently positioned and free of interpenetrations. Our framework satisfies these requirements, ensuring that the generated scenes are well-suited for reliable policy evaluation.

4.3 ABLATION STUDY

We first qualitatively illustrate the impact of our layout initialization module and simulation-in-the-loop optimization module. As shown in Figure 6(a), while the spatial relations between objects extracted directly from the depth map are generally reasonable, the scene still suffers from significant interpenetration: books intersecting with one another and the pen protruding its holder. By contrast, after applying our proposed layout initialization based on the scene tree, we obtain an intersection-free layout shown in Figure 6(b), where projections of each object along gravity direction typically lies in the projections of their containers or supporters, thereby satisfying physical dependency constraints along the gravity direction.

Nevertheless, simply enforcing physical dependencies before simulation does not ensure that the resulting simulated scene would still satisfy the intended semantics. In Figure 7(a), a stack of irregular blocks collapses after simulation due to an unbalanced center of mass. In contrast, Figure 7(b) demonstrates that, by further optimizing the initial layout through our simulation-in-the-loop optimization, the simulated scene converges to a stable configuration of stacked blocks that better reflects the semantics.

We further quantitatively evaluate the effectiveness of our method by computing semantic and physical metrics on both the depth-aligned layout without our layout initialization and optimization (denoted as *raw layout*), the layout from our scene initialization module (denoted as *Scene Init.*), and

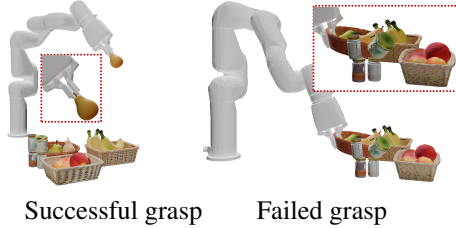


Figure 5: **Policy evaluation for robotic manipulation.** Example of a successful and a failed grasp where the attempted action causes objects to topple.

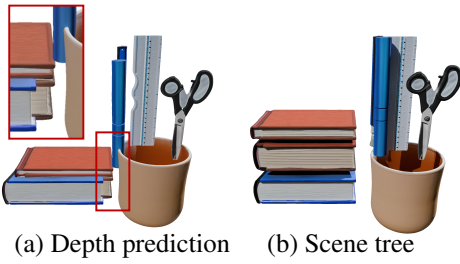


Figure 6: **Layout initialization w/o and w/ scene tree.** Layouts obtained from depth prediction (a) without and (b) with adjustment based on the scene tree. (Text prompt: “...a neatly stacked pile of three books...”. See Appendix D for the complete prompt.)

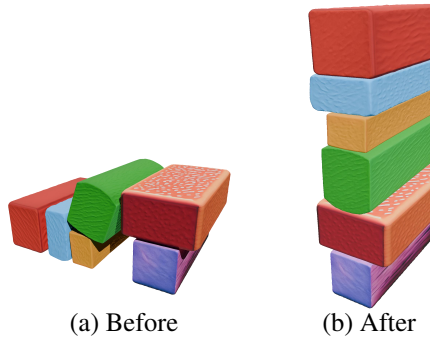


Figure 7: **Layout optimization.** Simulated layouts from initial layout (a) without and (b) with further optimization using differentiable simulation. (Text prompt: “a stack of colorful wooden blocks...”. See Appendix D for the complete prompt.)

compare them with our final output in Table 1. Our layout initialization removes penetration by sacrificing physical stability, but it enables applying our layout optimization to consistently improve all metrics. The gains in semantic consistency metrics are relatively smaller, as they primarily depend on visual appearance factors such as geometry and texture.

5 CONCLUSION

We presented **PAT3D**, a physics-augmented framework for text-to-3D scene generation that integrates vision-language reasoning with differentiable rigid body simulation. By decomposing the generation process into interpretable stages – object and relation extraction, layout initialization, and physics-guided layout optimization – our method produces 3D scenes that are not only semantically meaningful but also physically plausible and simulation-ready. Through extensive experiments on diverse, contact-rich scenes, we demonstrated that PAT3D achieves superior physical realism compared to existing approaches. We believe PAT3D represents a step forward in bridging high-level scene understanding with low-level physical reasoning. We hope this work inspires further research in physically grounded, controllable, and editable 3D scene generation.

Limitations and Future Work We present two representative failure cases in Figure 8 and Figure 9. While PAT3D handles most common physical dependencies, certain subtle relations remain challenging. In Figure 8, the concept of “hanging” in the prompt “A swing hanging from a tree” is misinterpreted, whereas a physically correct configuration would require the swing to be suspended from two specific attachment points. Extending our system to a broader set of spatial relations and larger-scale scenes are both promising directions for future work. One potential avenue is to incorporate path planning techniques and adopt a hierarchical optimization strategy to manage spatial complexity more effectively.



Figure 8: **Failure case 1.** Text prompt: “A swing hanging from a tree”. Figure 9: **Failure case 2.** Text prompt: “A brown leather sofa decorated with plush toys, ...”. See Appendix D for the complete prompt.



Our simulation-in-the-loop optimization is solved using a local optimizer. Although the objective reliably decreases, it does not guarantee convergence to the global optimum corresponding to perfect semantic alignment. This limitation appears in the failure case of Figure 9, where all stuffed toys should ideally rest on the sofa according to the prompt. However, due to the highly crowded configuration, the optimizer provides a suboptimal outcome: it reduces the number of fallen toys from three to one, yet one gray toy still remains on the floor. As the first work to incorporate differentiable simulation into 3D scene generation, we view the exploration of global optimization strategies as an exciting direction for future improvements, further expanding the possibilities opened by PAT3D.

REFERENCES

Aleksi Bochkovskii, Amaël Delaunoy, Hugo Germain, Marcel Santos, Yichao Zhou, Stephan R. Richter, and Vladlen Koltun. Depth pro: Sharp monocular metric depth in less than a second. In *International Conference on Learning Representations*, 2025. URL <https://arxiv.org/abs/2410.02073>.

Junhao Cai, Yuji Yang, Weihao Yuan, Yisheng He, Zilong Dong, Liefeng Bo, Hui Cheng, and Qifeng Chen. Gaussian-informed continuum for physical property identification and simulation. *arXiv e-prints*, pp. arXiv–2406, 2024.

Boyuan Chen, Hanxiao Jiang, Shaowei Liu, Saurabh Gupta, Yunzhu Li, Hao Zhao, and Shenlong Wang. Physgen3d: Crafting a miniature interactive world from a single image. *arXiv preprint arXiv:2503.20746*, 2025a.

Jinnan Chen, Lingting Zhu, Zeyu Hu, Shengju Qian, Yugang Chen, Xin Wang, and Gim Hee Lee. Mar-3d: Progressive masked auto-regressor for high-resolution 3d generation. *arXiv preprint arXiv:2503.20519*, 2025b.

Rui Chen, Yongwei Chen, Ningxin Jiao, and Kui Jia. Fantasia3d: Disentangling geometry and appearance for high-quality text-to-3d content creation. In *IEEE International Conference on Computer Vision (ICCV)*, 2023.

Yongwei Chen, Yushi Lan, Shangchen Zhou, Tengfei Wang, and Xingang Pan. Sar3d: Autoregressive 3d object generation and understanding via multi-scale 3d vqvae. *arXiv preprint arXiv:2411.16856*, 2024a.

Yongwei Chen, Tengfei Wang, Tong Wu, Xingang Pan, Kui Jia, and Ziwei Liu. Comboverse: Compositional 3d assets creation using spatially-aware diffusion guidance. In *European Conference on Computer Vision*, pp. 128–146. Springer, 2024b.

Yunuo Chen, Tianyi Xie, Zeshun Zong, Xuan Li, Feng Gao, Yin Yang, Ying Nian Wu, and Chenfanfu Jiang. Atlas3d: Physically constrained self-supporting text-to-3d for simulation and fabrication. *arXiv preprint arXiv:2405.18515*, 2024c.

Yu Fang, Minchen Li, Chenfanfu Jiang, and Danny M Kaufman. Guaranteed globally injective 3d deformation processing. *ACM Transactions on Graphics*, 40(4), 2021.

Gege Gao, Weiyang Liu, Anpei Chen, Andreas Geiger, and Bernhard Schölkopf. Graphdreamer: Compositional 3d scene synthesis from scene graphs. In *Proceedings of the IEEE/CVF Conference on Computer Vision and Pattern Recognition*, pp. 21295–21304, 2024.

Minghao Guo, Bohan Wang, Pingchuan Ma, Tianyuan Zhang, Crystal Owens, Chuang Gan, Josh Tenenbaum, Kaiming He, and Wojciech Matusik. Physically compatible 3d object modeling from a single image. *Advances in Neural Information Processing Systems*, 37:119260–119282, 2024.

Haonan Han, Rui Yang, Huan Liao, Jiankai Xing, Zunnan Xu, Xiaoming Yu, Junwei Zha, Xiu Li, and Wanhua Li. Reparo: Compositional 3d assets generation with differentiable 3d layout alignment. *arXiv preprint arXiv:2405.18525*, 2024.

Yicong Hong, Kai Zhang, Jiuxiang Gu, Sai Bi, Yang Zhou, Difan Liu, Feng Liu, Kalyan Sunkavalli, Trung Bui, and Hao Tan. Lrm: Large reconstruction model for single image to 3d. In *International Conference on Learning Representations (ICLR)*, 2024.

Yixin Hu, Teseo Schneider, Bolun Wang, Denis Zorin, and Daniele Panozzo. Fast tetrahedral meshing in the wild. *ACM Trans. Graph.*, 39(4), July 2020. ISSN 0730-0301. doi: 10.1145/3386569.3392385. URL <https://doi.org/10.1145/3386569.3392385>.

Kemeng Huang, Xinyu Lu, Huancheng Lin, Taku Komura, and Minchen Li. Stiffgipc: Advancing gpu ipc for stiff affine-deformable simulation, 2025. URL <https://arxiv.org/abs/2411.06224>.

Zehuan Huang, Yuan-Chen Guo, Xingqiao An, Yunhan Yang, Yangguang Li, Zi-Xin Zou, Ding Liang, Xihui Liu, Yan-Pei Cao, and Lu Sheng. Midi: Multi-instance diffusion for single image to 3d scene generation. *arXiv preprint arXiv:2412.03558*, 2024.

Tencent Hunyuan3D. Hunyuan3d 2.0: Scaling diffusion models for high resolution textured 3d assets generation, 2025.

Aaron Hurst, Adam Lerer, Adam P Goucher, Adam Perelman, Aditya Ramesh, Aidan Clark, AJ Os-trow, Akila Welihinda, Alan Hayes, Alec Radford, et al. Gpt-4o system card. *arXiv preprint arXiv:2410.21276*, 2024.

Minguk Kang, Jun-Yan Zhu, Richard Zhang, Jaesik Park, Eli Shechtman, Sylvain Paris, and Taesung Park. Scaling up gans for text-to-image synthesis. In *IEEE Conference on Computer Vision and Pattern Recognition (CVPR)*, 2023.

Diederik P Kingma. Adam: A method for stochastic optimization. *arXiv preprint arXiv:1412.6980*, 2014.

Alexander Kirillov, Eric Mintun, Nikhila Ravi, Hanzi Mao, Chloe Rolland, Laura Gustafson, Tete Xiao, Spencer Whitehead, Alexander C. Berg, Wan-Yen Lo, Piotr Dollár, and Ross Girshick. Segment anything. *arXiv:2304.02643*, 2023a.

Alexander Kirillov, Eric Mintun, Nikhila Ravi, Hanzi Mao, Chloe Rolland, Laura Gustafson, Tete Xiao, Spencer Whitehead, Alexander C Berg, Wan-Yen Lo, et al. Segment anything. In *Proceedings of the IEEE/CVF international conference on computer vision*, pp. 4015–4026, 2023b.

Lei Lan, Danny M. Kaufman, Minchen Li, Chenfanfu Jiang, and Yin Yang. Affine body dynamics: fast, stable and intersection-free simulation of stiff materials. *ACM Trans. Graph.*, 41(4), July 2022. ISSN 0730-0301.

Lei Lan, Minchen Li, Chenfanfu Jiang, Huamin Wang, and Yin Yang. Second-order stencil descent for interior-point hyperelasticity. *ACM Transactions on Graphics (TOG)*, 42(4):1–16, 2023.

Lei Lan, Zixuan Lu, Chun Yuan, Weiwei Xu, Hao Su, Huamin Wang, Chenfanfu Jiang, and Yin Yang. Jgs2: Near second-order converging jacobi/gauss-seidel for gpu elastodynamics. *ACM Trans. Graph.*, 44(4), July 2025. ISSN 0730-0301. doi: 10.1145/3731183. URL <https://doi.org/10.1145/3731183>.

Jiahao Li, Hao Tan, Kai Zhang, Zexiang Xu, Fujun Luan, Yinghao Xu, Yicong Hong, Kalyan Sunkavalli, Greg Shakhnarovich, and Sai Bi. Instant3d: Fast text-to-3d with sparse-view generation and large reconstruction model. In *International Conference on Learning Representations (ICLR)*, 2024.

Minchen Li, Zachary Ferguson, Teseo Schneider, Timothy R Langlois, Denis Zorin, Daniele Panozzo, Chenfanfu Jiang, and Danny M Kaufman. Incremental potential contact: intersection- and inversion-free, large-deformation dynamics. *ACM Trans. Graph.*, 39(4):49, 2020.

Minchen Li, Chenfanfu Jiang, Zhaofeng Luo, Wenxin Du, Chang Yu, Žiga Kovačič, and Tianyi Xie. *Physics-Based Simulation*. July 2025a. URL <https://phys-sim-book.github.io/>.

Qixuan Li, Chao Wang, Zongjin He, and Yan Peng. Phip-g: Physics-guided text-to-3d compositional scene generation. *arXiv preprint arXiv:2502.00708*, 2025b.

Xuan Li, Yu Fang, Lei Lan, Huamin Wang, Yin Yang, Minchen Li, and Chenfanfu Jiang. Subspace-preconditioned gpu projective dynamics with contact for cloth simulation. In *SIGGRAPH Asia 2023 Conference Papers*, pp. 1–12, 2023.

Chen-Hsuan Lin, Jun Gao, Luming Tang, Towaki Takikawa, Xiaohui Zeng, Xun Huang, Karsten Kreis, Sanja Fidler, Ming-Yu Liu, and Tsung-Yi Lin. Magic3d: High-resolution text-to-3d content creation. In *IEEE Conference on Computer Vision and Pattern Recognition (CVPR)*, 2023.

Zhiqiu Lin, Deepak Pathak, Baiqi Li, Jiayao Li, Xide Xia, Graham Neubig, Pengchuan Zhang, and Deva Ramanan. Evaluating text-to-visual generation with image-to-text generation, 2024. URL <https://arxiv.org/abs/2404.01291>.

Minghua Liu, Ruoxi Shi, Linghao Chen, Zhuoyang Zhang, Chao Xu, Xinyue Wei, Hansheng Chen, Chong Zeng, Jiayuan Gu, and Hao Su. One-2-3-45++: Fast single image to 3d objects with consistent multi-view generation and 3d diffusion. In *IEEE Conference on Computer Vision and Pattern Recognition (CVPR)*, 2024a.

Minghua Liu, Chao Xu, Haian Jin, Linghao Chen, Mukund Varma T, Zexiang Xu, and Hao Su. One-2-3-45: Any single image to 3d mesh in 45 seconds without per-shape optimization. In *Conference on Neural Information Processing Systems (NeurIPS)*, 2024b.

Ruoshi Liu, Rundi Wu, Basile Van Hoorick, Pavel Tokmakov, Sergey Zakharov, and Carl Vondrick. Zero-1-to-3: Zero-shot one image to 3d object. In *IEEE International Conference on Computer Vision (ICCV)*, 2023a.

Shaowei Liu, Zhongzheng Ren, Saurabh Gupta, and Shenlong Wang. Physgen: Rigid-body physics-grounded image-to-video generation. In *European Conference on Computer Vision*, pp. 360–378. Springer, 2024c.

Shilong Liu, Zhaoyang Zeng, Tianhe Ren, Feng Li, Hao Zhang, Jie Yang, Chunyuan Li, Jianwei Yang, Hang Su, Jun Zhu, et al. Grounding dino: Marrying dino with grounded pre-training for open-set object detection. *arXiv preprint arXiv:2303.05499*, 2023b.

Yuan Liu, Cheng Lin, Zijiao Zeng, Xiaoxiao Long, Lingjie Liu, Taku Komura, and Wenping Wang. Syncdreamer: Generating multiview-consistent images from a single-view image. In *International Conference on Learning Representations (ICLR)*, 2024d.

Xiaoxiao Long, Yuan-Chen Guo, Cheng Lin, Yuan Liu, Zhiyang Dou, Lingjie Liu, Yuexin Ma, Song-Hai Zhang, Marc Habermann, Christian Theobalt, et al. Wonder3d: Single image to 3d using cross-domain diffusion. In *IEEE Conference on Computer Vision and Pattern Recognition (CVPR)*, 2024.

Gal Metzer, Elad Richardson, Or Patashnik, Raja Giryes, and Daniel Cohen-Or. Latent-nerf for shape-guided generation of 3d shapes and textures. In *IEEE Conference on Computer Vision and Pattern Recognition (CVPR)*, 2023.

Oscar Michel, Roi Bar-On, Richard Liu, Sagie Benaim, and Rana Hanocka. Text2mesh: Text-driven neural stylization for meshes. In *IEEE Conference on Computer Vision and Pattern Recognition (CVPR)*, 2022.

Siddharth Ahuja or ahujasid. blender-mcp: Blender model context protocol integration. <https://github.com/ahujasid/blender-mcp>, 2025. Accessed: YYYY-MM-DD.

A Paszke. Pytorch: An imperative style, high-performance deep learning library. *arXiv preprint arXiv:1912.01703*, 2019.

Ben Poole, Ajay Jain, Jonathan T Barron, and Ben Mildenhall. Dreamfusion: Text-to-3d using 2d diffusion. In *International Conference on Learning Representations (ICLR)*, 2023.

Alec Radford, Jong Wook Kim, Chris Hallacy, Aditya Ramesh, Gabriel Goh, Sandhini Agarwal, Girish Sastry, Amanda Askell, Pamela Mishkin, Jack Clark, Gretchen Krueger, and Ilya Sutskever. Learning transferable visual models from natural language supervision, 2021. URL <https://arxiv.org/abs/2103.00020>.

Aditya Ramesh, Prafulla Dhariwal, Alex Nichol, Casey Chu, and Mark Chen. Hierarchical text-conditional image generation with clip latents. *arXiv preprint arXiv:2204.06125*, 1(2):3, 2022.

Tianhe Ren, Shilong Liu, Ailing Zeng, Jing Lin, Kunchang Li, He Cao, Jiayu Chen, Xinyu Huang, Yukang Chen, Feng Yan, Zhaoyang Zeng, Hao Zhang, Feng Li, Jie Yang, Hongyang Li, Qing Jiang, and Lei Zhang. Grounded sam: Assembling open-world models for diverse visual tasks, 2024.

Robin Rombach, Andreas Blattmann, Dominik Lorenz, Patrick Esser, and Björn Ommer. High-resolution image synthesis with latent diffusion models. In *IEEE Conference on Computer Vision and Pattern Recognition (CVPR)*, 2022.

Ruoxi Shi, Hansheng Chen, Zhuoyang Zhang, Minghua Liu, Chao Xu, Xinyue Wei, Linghao Chen, Chong Zeng, and Hao Su. Zero123++: a single image to consistent multi-view diffusion base model. *arXiv preprint arXiv:2310.15110*, 2023.

Yichun Shi, Peng Wang, Jianglong Ye, Mai Long, Kejie Li, and Xiao Yang. Mvdream: Multi-view diffusion for 3d generation. In *International Conference on Learning Representations (ICLR)*, 2024.

Jaidev Shriram, Alex Trevithick, Lingjie Liu, and Ravi Ramamoorthi. Realmdreamer: Text-driven 3d scene generation with inpainting and depth diffusion. *arXiv preprint arXiv:2404.07199*, 2024.

Jingxiang Sun, Bo Zhang, Ruizhi Shao, Lizhen Wang, Wen Liu, Zhenda Xie, and Yebin Liu. Dreamcraft3d: Hierarchical 3d generation with bootstrapped diffusion prior. In *International Conference on Learning Representations (ICLR)*, 2024.

Yifan Sun, Menglin Zhang, Yi Jiang, Xinyu Wang, Kai Chen, Ping Luo, and Dahua Lin. Layoutvlm: Indoor scene layout generation with vision-language models. In *IEEE Conference on Computer Vision and Pattern Recognition (CVPR)*, 2025.

Dmitry Tochilkin, David Pankratz, Zexiang Liu, Zixuan Huang, , Adam Letts, Yangguang Li, Ding Liang, Christian Laforte, Varun Jampani, and Yan-Pei Cao. Triposr: Fast 3d object reconstruction from a single image. *arXiv preprint arXiv:2403.02151*, 2024.

Alexander Vilesov, Pradyumna Chari, and Achuta Kadambi. Cg3d: Compositional generation for text-to-3d via gaussian splatting. *arXiv preprint arXiv:2311.17907*, 2023.

Haochen Wang, Xiaodan Du, Jiahao Li, Raymond A Yeh, and Greg Shakhnarovich. Score jacobian chaining: Lifting pretrained 2d diffusion models for 3d generation. In *IEEE International Conference on Computer Vision (ICCV)*, 2023.

Peng Wang and Yichun Shi. Imagedream: Image-prompt multi-view diffusion for 3d generation. *arXiv preprint arXiv:2312.02201*, 2023.

Xinjie Wang, Liu Liu, Yu Cao, Ruiqi Wu, Wenkang Qin, Dehui Wang, Wei Sui, and Zhizhong Su. Embodiedgen: Towards a generative 3d world engine for embodied intelligence, 2025. URL <https://arxiv.org/abs/2506.10600>.

Zhengyi Wang, Cheng Lu, Yikai Wang, Fan Bao, Chongxuan Li, Hang Su, and Jun Zhu. Prolific-dreamer: High-fidelity and diverse text-to-3d generation with variational score distillation. In *Conference on Neural Information Processing Systems (NeurIPS)*, 2024.

Dejia Xu, Hanwen Liang, Neel P Bhatt, Hezhen Hu, Hanxue Liang, Konstantinos N Plataniotis, and Zhangyang Wang. Comp4d: Llm-guided compositional 4d scene generation. *arXiv preprint arXiv:2403.16993*, 2024a.

Yinghao Xu, Hao Tan, Fujun Luan, Sai Bi, Peng Wang, Jiahao Li, Zifan Shi, Kalyan Sunkavalli, Gordon Wetzstein, Zexiang Xu, and Kai Zhang. Dmv3d: Denoising multi-view diffusion using 3d large reconstruction model. In *International Conference on Learning Representations (ICLR)*, 2024b.

Han Yan, Mingrui Zhang, Yang Li, Chao Ma, and Pan Ji. Phycage: Physically plausible compositional 3d asset generation from a single image. *arXiv preprint arXiv:2411.18548*, 2024.

Kaixin Yao, Longwen Zhang, Xinhao Yan, Yan Zeng, Qixuan Zhang, Lan Xu, Wei Yang, Jiayuan Gu, and Jingyi Yu. Cast: Component-aligned 3d scene reconstruction from an rgb image. *arXiv preprint arXiv:2502.12894*, 2025.

Jiahui Yu, Yuanzhong Xu, Jing Yu Koh, Thang Luong, Gunjan Baid, Zirui Wang, Vijay Vasudevan, Alexander Ku, Yinfei Yang, Burcu Karagol Ayan, et al. Scaling autoregressive models for content-rich text-to-image generation. In *International Conference on Machine Learning (ICML)*, 2022.

Tianyuan Zhang, Hong-Xing Yu, Rundi Wu, Brandon Y Feng, Changxi Zheng, Noah Snavely, Jiajun Wu, and William T Freeman. Physdreamer: Physics-based interaction with 3d objects via video generation. In *European Conference on Computer Vision*, pp. 388–406. Springer, 2024.

Haoyu Zhao, Hao Wang, Xingyue Zhao, Hongqiu Wang, Zhiyu Wu, Chengjiang Long, and Hua Zou. Automated 3d physical simulation of open-world scene with gaussian splatting. *arXiv preprint arXiv:2411.12789*, 2024.

Xiaoyu Zhou, Xingjian Ran, Yajiao Xiong, Jinlin He, Zhiwei Lin, Yongtao Wang, Deqing Sun, and Ming-Hsuan Yang. Gala3d: Towards text-to-3d complex scene generation via layout-guided generative gaussian splatting. *arXiv preprint arXiv:2402.07207*, 2024.

Yang Zhou, Zongjin He, Qixuan Li, and Chao Wang. Layoutdreamer: Physics-guided layout for text-to-3d compositional scene generation. *arXiv preprint arXiv:2502.01949*, 2025.

Zhizhuo Zhou and Shubham Tulsiani. Sparsefusion: Distilling view-conditioned diffusion for 3d reconstruction. In *IEEE Conference on Computer Vision and Pattern Recognition (CVPR)*, 2023.

A PSEUDO-CODE OF BUILDING SCENE TREE

Algorithm 1 Build Scene Tree

Require:

Scene objects \mathcal{O}

Root node \mathcal{G} (ground)

Ensure:

Hierarchical scene tree \mathcal{T} ;

- 1: Initialize tree \mathcal{T} with root node \mathcal{G} ;
- 2: Mark all objects in \mathcal{O} as unvisited;
- 3: **Procedure** BuildSceneTree(n):
- 4: **for** $o \in \mathcal{O}$ where o is unvisited **do**
- 5: **if** o is in contact with n **and** o has an physical dependency relation with n **then**
- 6: Add o as a child of n in \mathcal{T} ;
- 7: Mark o as visited;
- 8: **Call** BuildSceneTree(o);
- 9: **end if**
- 10: **end for**
- 11: **Call** BuildSceneTree(\mathcal{G});

B DIFFERENTIABLE SIMULATION DETAILS

B.1 FORWARD SIMULATION

We model each object in the scene as a stiff affine body Lan et al. (2022), where any point on the object with an initial position $\bar{\mathbf{x}}_{\text{init}}$ undergoes an affine transformation to its current position $\mathbf{x} = \mathbf{A}\bar{\mathbf{x}}_{\text{init}} + \mathbf{p}$, where $\mathbf{A} \in \mathbb{R}^{3 \times 3}$ is a transformation matrix and \mathbf{p} is a translation vector. Together, they define the degrees of freedom (DOFs) of the object as $\mathbf{q} \equiv [\mathbf{p}, \mathbf{A}] \in \mathbb{R}^{3 \times 4}$.

To simulate the motion and contact of the objects, we employ a custom GPU-optimized affine body dynamics (ABD) simulator based on Huang et al. (2025). The simulator solves for the configuration $q_{n+1} \in \mathbb{R}^{12N}$ at time step $n+1$, formed by flattening and stacking the DOFs of all N objects, from the configuration q_n at the previous time step via:

$$M(q_{n+1} - \tilde{q}_n) + \Delta t^2 (\nabla \Psi(q_{n+1}) + \nabla B(q_{n+1}) + \nabla D(q_{n+1}, q_n)) = 0. \quad (4)$$

Here, M is the mass matrix, and $\tilde{q}_n = q_n + \Delta t^2 g$ is the predictive state used in artificial time stepping, which omits velocity. Δt denotes the simulation time step, and g is the gravitational acceleration. The potential Ψ models stiff elasticity to preserve object shape, B is a barrier potential enforcing non-penetration constraints, and D is a semi-implicit friction potential following Li et al. (2020). See more details in Li et al. (2025a).

B.2 BACKPROPAGATION

To optimize the initial layout q_0 , we compute the gradient of the loss function L w.r.t q_0 using the chain rule:

$$\frac{dL}{dq_0} = \left(\frac{\partial q_1}{\partial q_0} \right)^\top \left(\frac{\partial q_2}{\partial q_1} \right)^\top \dots \left(\frac{\partial q_n}{\partial q_{n-1}} \right)^\top \left(\frac{\partial q_{n+1}}{\partial q_n} \right)^\top \frac{dL}{dq_{n+1}}. \quad (5)$$

Here, $\frac{dL}{dq_{n+1}}$ can be directly computed at the target step $n+1$ or automatically obtained via PyTorch Paszke (2019). The key step lies in computing $\frac{\partial q_{n+1}}{\partial q_n}$, which we derive using implicit differentiation. Rewriting Equation 4 yields:

$$q_{n+1} = q_n + \Delta t^2 M^{-1} [f(q_{n+1}) + Mg], \quad (6)$$

where $f(q_{n+1}) = -\nabla \Psi(q_{n+1}) - \nabla B(q_{n+1}) - \nabla_{q_{n+1}} D(q_{n+1}, q_n)$. Differentiating both sides of Equation 6 with respect to q_n and isolating the derivative yields:

$$\frac{\partial q_{n+1}}{\partial q_n} = \left[I - \Delta t^2 M^{-1} \frac{\partial f(q_{n+1})}{\partial q_{n+1}} \right]^{-1} \left[I - \Delta t^2 M^{-1} \frac{\partial^2 D(q_{n+1}, q_n)}{\partial q_{n+1} \partial q_n} \right]^{-1}. \quad (7)$$

Substituting Equation 7 into the chain rule expression in Equation 5 allows us to compute the full gradient $\frac{dl}{dq_0}$, which we use to update the initial layout. Both forward simulation and backpropagation are fully GPU-accelerated for computational efficiency.

B.3 PHYSICAL AND ALGORITHMIC PARAMETERS

All simulations are performed using our differentiable rigid body simulator with the following physical and algorithmic parameters. They are generally applicable to rigid body scenes and only a few of them needs tuning. We define the mms, i.e. the mean mesh size, to be the average of the longest side of the bounding box of all meshes.

Fixed parameters:

- **Friction coefficient:** A Coulomb friction coefficient of 0.2 is used for all contact interactions.
- **Normal contact stiffness:** The penalty-based normal-force model uses an effective stiffness of 1.0 GPa, corresponding to rigid-body behavior.
- **Gravity:** Standard Earth gravity $\mathbf{g} = (0, -9.8, 0) \text{ m s}^{-2}$ is used.
- **Time step (Δt):** The simulation is integrated using a time step of 0.03 s.
- **Newton solver tolerance:** In each time step, Newton’s method is applied to solve the time integration problem, and the termination criteria is the velocity residual falls below 0.1 m s^{-1} .
- **Maximum number of frames:** This specifies the duration of the simulation. We use 300 frames for all the scenes.
- **Optimization learning rate:** We use a learning rate of 0.001 for simulation-in-the-loop optimization.
- **Maximum optimization epochs:** Differentiable simulation is allowed up to 50 optimization iterations.

Tunable parameters:

- **Contact distance threshold:** A threshold of 0.01mms is used for collision handling in most cases. Two objects are considered in contact when their distance falls below this value. We use a value of 5×10^{-4} for the stackedblocks scene to capture the intricate balancing behavior.
- **Friction velocity threshold:** Relative velocities below 0.01mms are modeled to generate static friction forces for most cases. We use a value of 10^{-5} for the stacked blocks scene.
- **Optimization frame interval:** We compute semantic losses every 10 frames by default and accumulate it during the simulation. This parameter are set according to the frequency of contact events in each simulation. Most of our examples achieve perfect semantic alignment at the first optimization iteration, and thus no tuning needed.

B.4 TIMING AND MEMORY CONSUMPTION

All experiments are conducted on a single NVIDIA A5000 GPU. The average end-to-end time to generate a scene is 1632 seconds. The main computational cost arises from object generation, which requires an average of 762 seconds per scene. During the simulation-in-the-loop stage, each optimization iteration takes approximately 30 seconds, and we use 50 iterations in total, selecting the solution with the lowest objective value.

For all generated scenes, the simulation fits within 8 GB of GPU memory. In practice, memory usage scales with the size of the contact graph, which depends on the geometric complexity of the objects and the number of active contacts in the scene. Our formulation relies on sparse matrix representations for both system dynamics and contact operators, which helps maintain a moderate memory footprint.

Given ongoing improvements in GPU hardware and simulation techniques Li et al. (2023); Lan et al. (2023; 2025), we do not anticipate efficiency and memory to be the limiting factors for typical applications.

C IMPLEMENTATION DETAILS

We implement our proposed algorithm in Python on Ubuntu 20.04. In the layout optimization, we leverage Libupic Huang et al. (2025) as a simulation platform. The optimization is performed using ADAM Kingma (2014). Scenes that are already semantically consistent after the first simulation are not optimized. Our algorithm is deployed and run on a single NVIDIA RTX 4090 GPU. All our baselines were tested on the NVIDIA A6000 GPU.

D TEXT PROMPT USED IN ABLATION STUDY

The complete text prompt used in our ablation study are as follows.

- Figure 6: “*On the left side, there is a metallic cylindrical pen holder containing two black pens, a wooden ruler, and a pair of gray-handled scissors. On the right side, there is a neatly stacked pile of three books with red covers and visible pages. The items are placed on a light wooden surface, and the background is plain white, creating a bright and simple composition.*”
- Figure 7: “*a stack of colorful wooden blocks arranged vertically, featuring red, blue, yellow, green, orange, and purple pieces, balanced on a flat surface.*”.
- Figure 9 “*A brown leather sofa decorated with plush toys, including two large teddy bears, a gray elephant, a white rabbit, a yellow giraffe, and two throw pillows, sits in a cozy room with two round burgundy floor cushions in front.*”

E MORE EXAMPLES

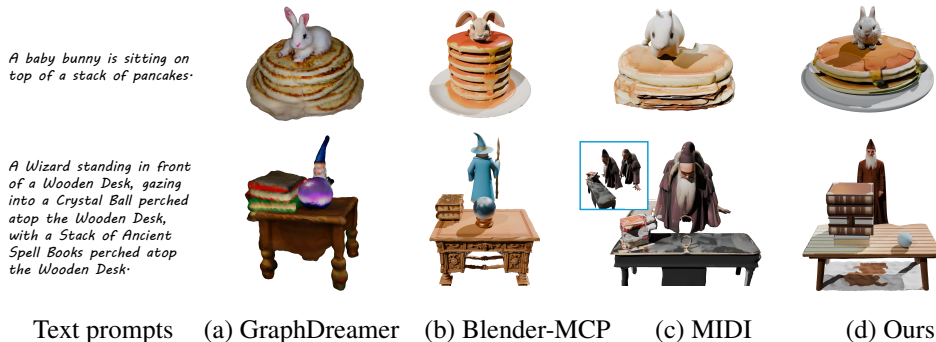


Figure 10: **Comparison of generated scenes from text prompts used in GraphDreamer Gao et al. (2024).**

In addition to the 18 text prompts used for comparison with the baseline, we further tested our algorithm on 12 additional examples, as shown in Figure 12. All of these prompts yielded semantically accurate and physically stable results.

F METIRCS

Clip score and VQAScore These two metrics measure the semantic similarity between the rendered scene images and the corresponding input text prompt. Specifically, we render the scene from 18 viewpoints by sampling three depression angles (0° , 20° , and 45°) and six evenly distributed horizontal angles. These rendered images are then used to compute the Clip score and VQAScore.

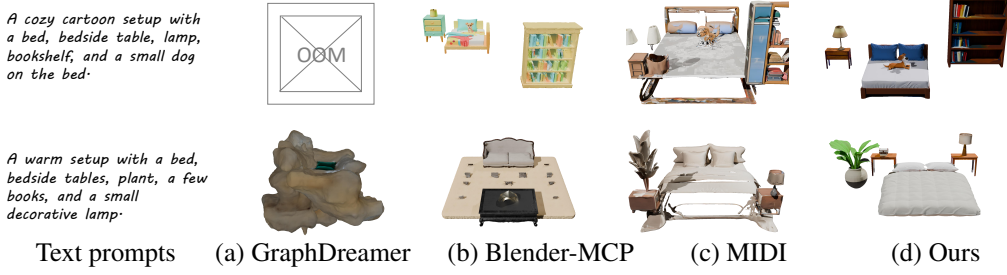


Figure 11: **Comparison of generated scenes from text prompts used in MIDI Huang et al. (2024).**

Simulated Scene Displacement (D) This metric computes the normalized average displacement of object vertices in the scene before and after applying a simulation. To ensure consistency across different baselines, we first normalize all scenes such that their bounding box diagonal length equals 2. We then compute the displacement of every vertex over all simulated frames and aggregate these values into a single scalar quantity. Finally, this scalar is normalized by the total number of vertices and by the scene’s diagonal length. Formally, let $v_j^{(t)}$ denote the position of vertex j at simulation frame t , and let V and T denote the number of vertices and frames, respectively. The metric is defined as the average per-vertex displacement normalized by the scene diagonal length l :

$$D = \frac{1}{Vl} \sum_{j=1}^V \sum_{t=1}^T \|v_j^{(t)} - v_j^{(t-1)}\|, \quad (8)$$

Ratio of Penetrating Triangle Pairs (R) This metric quantifies the extent of penetration between objects in the scene, serving as an indicator of the scene’s geometric correctness. We first normalize all scenes such that their bounding box diagonal length equals 2. We then remesh each object using fTetWild Hu et al. (2020), setting the target triangle edge length to 0.05 times the scene diagonal. After normalization, we compute R as the ratio between an approximated total length of intersection contours and the length of the scene diagonal l : $R = \frac{(T_p - \sum_{i=1}^N T_{p,i})l_e}{l}$, where T_p is the total number of penetrating triangle pairs in the scene, $T_{p,i}$ is the number of self-penetrating triangle pairs in object i , which is excluded, and l_e is the average edge length of all object meshes.

Physical Plausibility Score This VLM-based metric evaluates the physical plausibility of a generated scene by asking a GPT model to score the realism of object contacts and physical relationships in the rendered image. Specifically, we use the following prompt:

“The semantic meaning of this scene is: ‘...’. Please evaluate whether the physical relationships in this image are reasonable and whether the contacts between objects are physically realistic. Give this scene a physical plausibility score from 0 to 100.”

G MORE COMPARISON

We qualitatively compare our method with the baselines on the text prompts previously presented in MIDI and GraphDreamer, as shown in Figure 11 and Figure 10, respectively. For the comparison with MIDI, since it requires an image as input, we first generate images from the provided text prompts in their paper and use these as MIDI’s inputs. For the other baselines, we directly use the text prompts. For our method, we use the same text prompts while ensuring that the reference image is consistent with the input image used for MIDI.



"A silver laptop with its screen turned off is placed on a small round wooden stool with three legs."



"A table with a basket of eggs on it."



"A small inflatable blue-and-white kiddie pool is filled with eight colorful beach balls with red, yellow, and white panels float on the surface. ."



"A round white plate holds a simple arrangement of food: two brown sausages placed side by side, several pieces of bright yellow corn on the cob cut into chunks, and three green broccoli florets."



"Four woven baskets arranged in a row, each containing different fruit: pears, bananas, oranges, and apples, alongside two stacks of jam jars."



"There is a white cylindrical holder containing several stationery items, including a pair of black-handled scissors, a white ruler, a blue pen, and a mechanical pencil. To its left lies a neatly stacked pile of three hardcover books in earthy tones of orange, beige, and blue."



"A transparent glass mug supports a stack of two beige bowls and two beige plates, with a silver fork standing upright on the topmost plate."



"On the desk, a black desk lamp sits on the left, accompanied by a white mug filled with pencils. The right side is dominated by a tall stack of hardcover books, with an open book on top, while a small potted plant adds a touch of greenery on the far right. A black leather office chair is centered behind the desk."



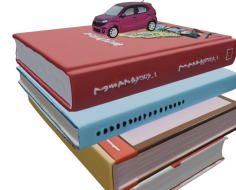
"A small chocolate cake topped with a swirl of white whipped cream and decorated with two fresh red strawberries, served on a round white plate placed on a wooden table."



"A fruit basket containing one banana and two apples."



"An inflatable swimming pool with toy ducks, a boat, and a starfish toy."



"A toy car on four books."

Figure 12: More results of our method.